Vol 459|7 May 2009|doi:10.1038/nature07883

LETTERS

Fused has evolved divergent roles in vertebrate Hedgehog signalling and motile ciliogenesis

Christopher W. Wilson[1]*, Catherine T. Nguyen[2]*, Miao-Hsueh Chen[1], Jehn-Hsiahn Yang[1]†, Rhodora Gacayan[1], Jie Huang[2], Jau-Nian Chen[2] & Pao-Tien Chuang[1]

Hedgehog (Hh) signalling is essential for several aspects of embryogenesis[1,2]. In *Drosophila*, Hh transduction is mediated by a cytoplasmic signalling complex[3–5] that includes the putative serine-threonine kinase Fused (Fu) and the kinesin Costal 2 (Cos2, also known as Cos), yet Fu does not have a conserved role in Hh signalling in mammals[6,7]. Mouse *Fu* (also known as *Stk36*) mutants are viable and seem to respond normally to Hh signalling. Here we show that mouse Fu is essential for construction of the central pair apparatus of motile, 9+2 cilia and offers a new model of human primary ciliary dyskinesia. We found that mouse Fu physically interacts with Kif27, a mammalian Cos2 orthologue[8], and linked Fu to known structural components of the central pair apparatus, providing evidence for the first regulatory component involved in central pair construction. We also demonstrated that zebrafish Fu is required both for Hh signalling and cilia biogenesis in Kupffer's vesicle. Mouse Fu rescued both Hh-dependent and -independent defects in zebrafish. Our results delineate a new pathway for central pair apparatus assembly, identify common regulators of Hh signalling and motile ciliogenesis, and provide insights into the evolution of the Hh cascade.

To further investigate the role of Fu in mammalian Hh signalling, we addressed whether Hh-dependent Smo localization to the primary cilium is affected in the absence of Fu. Primary cilia, which have a '9+0' arrangement of nine outer doublet microtubules, are required for Hh responses and contain several Hh pathway components[2,9]. We found that $Fu^{-/-}$ mouse embryonic fibroblasts formed primary cilia normally, trafficked Smo to the primary cilium in response to Hh ligand, and exhibited a typical Gli transcriptional response (Supplementary Figs 1, 2 and data not shown). This suggests that the single mammalian *Fu* orthologue is dispensable for Hh signalling. To explore the function of *Fu* in mice, we examined its expression in postnatal tissues by *in situ* hybridization. The *Fu* transcript was strongly expressed in the respiratory epithelium, the ependymal lining of the ventricles in the brain, and in the oviduct and testis (Fig. 1a–c and data not shown). These expression patterns are reminiscent of genes involved in the biogenesis of motile cilia, which function in these tissues to propel mucus, fluid and cells. In contrast to the primary cilium, the classical '9+2' motile cilium consists of nine outer doublet microtubules and two singlet central pair microtubules[10]. The central pair apparatus has a crucial involvement in regulating ciliary motility, but its formation is poorly understood because the centriole-derived basal body, from which the cilia axoneme extends, does not provide a template for central pair outgrowth. Disruption of human motile cilia function leads to primary ciliary dyskinesia, which is associated with recurrent respiratory infection, hydrocephalus and infertility[11–13]. To determine whether motile cilia function is compromised in $Fu^{-/-}$ mice, we studied cilia axonemal ultrastructure by transmission electron microscopy. In wild-type animals, over 99% of tracheal and ependymal motile cilia showed a typical 9+2 configuration (Fig. 1d, f and Supplementary Figs 3 and 4). In contrast, approximately 60% of $Fu^{-/-}$ cilia have abnormal ciliary ultrastructure; two-thirds of which lack the central pair apparatus (Fig. 1e, f and Supplementary Figs 3 and 4). Central pair defects in *Fu* mutants are apparent at the basal plate region characterized by an electron-dense thick band, where the central pair originates in wild-type cilia[14] (Supplementary Fig. 4). Our findings indicate that mammalian *Fu* is dispensable for Hh signalling and specifically participates in the generation of the central pair apparatus in motile cilia axonemes.

Mice lacking functional *Fu* are born with no obvious phenotype, but they fail to thrive in comparison with wild-type or heterozygous littermates and die before postnatal day (P) 21 (refs 6, 7). To determine the functional consequences of central pair apparatus loss in $Fu^{-/-}$ animals, we examined fluid flow in tracheal explants. Analysis of fluorescent bead movement showed strong distal–proximal directional flow in wild-type explants, whereas beads overlaid on $Fu^{-/-}$ tracheae showed severely impaired velocity and little to no directional movement (Fig. 1g–i and Supplementary Movies 1 and 2). We next determined whether elimination of the central pair apparatus in $Fu^{-/-}$ animals disrupted cilia motion. In wild-type tracheae, cilia beat in a linear path with a quick forward power stroke and a slower recovery stroke[15] (Fig. 1j and Supplementary Movies 3 and 5). Most $Fu^{-/-}$ cilia moved stiffly and had a markedly reduced stroke amplitude; a subset were either immotile or beat in a slow, circular motion (Fig. 1k and Supplementary Movies 4 and 6). In contrast to wild-type motile cilia, which beat coordinately to produce a metachronic wave[16], cilia in $Fu^{-/-}$ animals that beat seemed disoriented with respect to their neighbours (Fig. 1k and Supplementary Movies 4 and 6). This prompted us to investigate whether cilia orientation, specified by a basal body accessory structure known as the basal foot, was perturbed[17,18]. In wild-type tracheae, basal feet were properly aligned with each other (Fig. 1m). In $Fu^{-/-}$ mutants, basal feet were disoriented and frequently pointed at right angles or antiparallel to one another (Fig. 1n), and the circular standard deviation of cilia orientation within a given cell was significantly higher (Fig. 1l). Loss of the central pair apparatus in $Fu^{-/-}$ mice thus eliminated directional fluid flow, resulting from uncoordinated ciliary beating and global disorganization of cilia polarity.

We proposed that Fu in different metazoan species might participate in both Hh signalling and ciliogenesis. We examined the role of Fu in zebrafish because *fu* (also known as *stk36*) morphants exhibit mild Hh-dependent somite phenotypes[19]. By delivering a higher concentration of *fu* morpholino, we observed stronger Hh phenotypes, including

[1]Cardiovascular Research Institute, University of California, San Francisco, California 94158, USA. [2]Department of Molecular, Cell and Developmental Biology, University of California, Los Angeles, California 90095, USA. †Present address: Department of Obstetrics and Gynecology, College of Medicine and the Hospital, National Taiwan University, Taipei, Taiwan. *These authors contributed equally to this work.

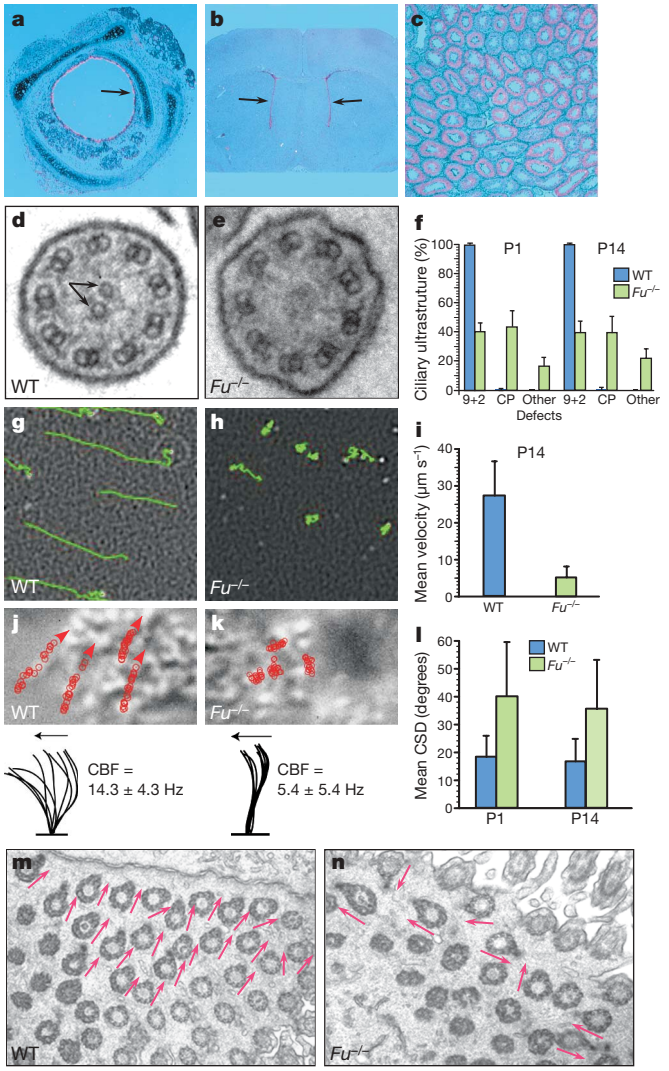

Figure 1 | Mouse *Fu* is required for central pair apparatus construction. **a–c**, Expression of *Fu* (pink signal) in the mouse tracheal epithelium (**a**), ependyma of the lateral ventricles (**b**), and testis (**c**) at P14 by section *in situ* hybridization to *Fu*. Arrows indicate sites of *Fu* expression. **d, e**, Transmission electron micrographs of motile cilia from wild-type (WT) and $Fu^{-/-}$ tracheae. Arrows denote the central pair microtubules. **f**, Quantification of ultrastructural defects from P1 and P14 tracheae (P1: $n = 4$ animals (wild type and $Fu^{-/-}$), mean cilia per animal analysed = 88 (wild type) and 64 ($Fu^{-/-}$); P14: $n = 7$ (wild type) and $n = 6$ ($Fu^{-/-}$), mean cilia per animal analysed = 113 (wild type) and 93 ($Fu^{-/-}$)). CP, central pair. Error bars indicate s.d. **g, h**, Traces of fluorescent-bead movement over tracheal explants. **i**, Mean particle velocity in P14 wild-type ($n = 5$) and $Fu^{-/-}$ ($n = 5$) tracheae. Error bars indicate s.d. **j, k**, Traces of cilia beat path overlaid on still differential interference contrast (DIC) images of tracheal cilia (top panels) and lateral traces of cilia waveform (bottom panels). Mean ciliary beat frequency (CBF) was calculated from 30 cilia ($n = 3$ animals for wild type and $Fu^{-/-}$). Arrows indicate directions of the forward effective strokes. **l**, Quantification of circular standard deviation (CSD) of basal feet from P1 (wild type, $n = 24$ cells from four animals; $Fu^{-/-}$, $n = 38$ cells from four animals; $P < 3.4 \times 10^{-6}$; unpaired Student's *t*-test) and P14 (wild type, $n = 31$ cells from four animals; $Fu^{-/-}$, $n = 36$ cells from three animals; $P < 2.6 \times 10^{-7}$; unpaired Student's *t*-test). Error bars indicate s.d. **m, n**, Representative transmission electron micrographs images of basal foot polarity (arrows) in P14 wild-type and $Fu^{-/-}$ tracheae. Original magnification, ×40 (**a–c**), ×44,000 (**d, e**), ×400 (**g, h**), ×900 (**j, k**) and ×26,500 (**m, n**).

cyclopia and loss of lateral floor plate (Fig. 2a, b, d, e, Supplementary Fig. 5 and data not shown), similar to *smo* mutants[20]. Knockdown of zebrafish *fu* activity greatly reduced *patched1* (*ptc1*) expression in somites, suggesting disruption of Hh responses (Fig. 2g, h). The

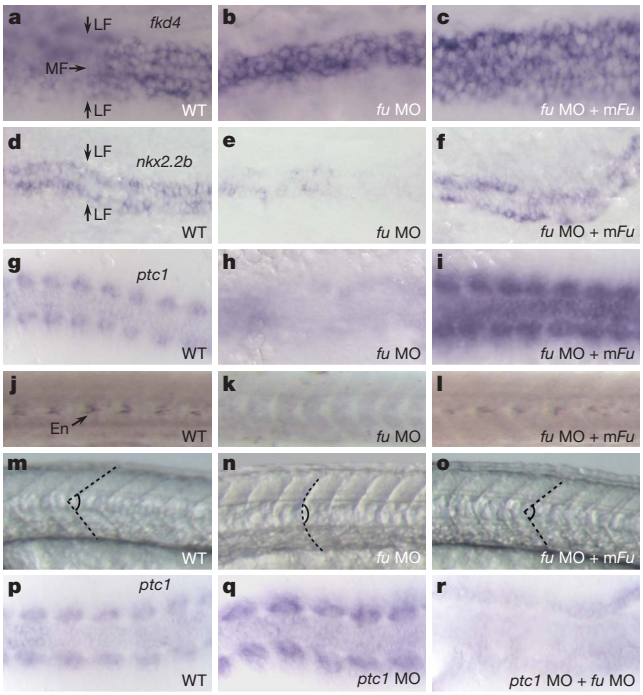

Figure 2 | Mouse *Fu* is capable of rescuing Hh-related phenotypes in zebrafish *fu* morphants. **a**, Whole-mount *in situ* hybridization to *fkd4* (also known as *foxa*; purple signal) in both medial and lateral floor plate of wild-type (WT) zebrafish embryos at 24 h post fertilization (h.p.f.). **b, c**, *fkd4* expression is lost in the lateral floor plate of *fu* morphants (MO) (**b**) and is restored when mouse *Fu* is expressed (**c**). **d**, Whole-mount *in situ* hybridization to *nkx2.2b* (purple signal) in the lateral floor plate of wild-type zebrafish embryos at 24 h.p.f. **e, f**, *nkx2.2b* expression is lost in the lateral floor plate of *fu* morphants (**d**) and is restored when mouse *Fu* is expressed (**e**). View is dorsal. LF, lateral floor plate; MF, medial floor plate. **g**, Whole-mount *in situ* hybridization to *ptc1* (purple signal) in somites of wild-type zebrafish embryos at the 10-somite stage. View is dorsal. **h, i**, *ptc1* expression is greatly reduced in somites of *fu* morphants (**h**) and is restored when mouse *Fu* is expressed (**i**). **j**, Immunohistochemistry against Eng1a and Eng1b (En) (arrow), which labels the muscle pioneer population in wild-type zebrafish somites at 24 h.p.f. View is lateral. **k, l**, Rescue of En expression in *fu* morphant somites (**k**) by co-injection with mouse *Fu* (**l**). **m**, Lateral view of chevron-shaped somites in wild-type zebrafish embryos at 24 h.p.f. **n, o**, Rescue of U-shaped somites in *fu* morphants (**n**) by co-injection with mouse *Fu* (**o**). Dotted lines delineate the boundaries of somites. **p**, Whole-mount *in situ* hybridization to *ptc1* (purple signal) in somites of wild-type zebrafish embryos at the 10-somite stage. View is dorsal. **q, r**, Upregulation of *ptc1* expression in *ptc1* morphants (**q**) is abolished by knocking down *fu* (**r**). Original magnification, ×200 (**a–i, p–r**), ×105.6 (**j–l**) and ×64 (**m–o**).

Hh-dependent muscle pioneer population, marked by the expression of *engrailed 1a* and *1b* (*eng1a and eng1b*), was lost (Fig. 2j, k), and *fu* morphants developed U-shaped instead of chevron-shaped somites (Fig. 2m, n). In *ptc1* morphants, Hh target genes are upregulated cell autonomously (Fig. 2p, q and Supplementary Fig. 10)[19]. Upregulation of Hh target genes is abolished in *ptc1*;*fu* double morphants (Fig. 2r), indicating that *fu* functions cell autonomously in Hh-responsive cells to control Hh signalling. Taken together, these results provide convincing evidence for an integral role of Fu in the zebrafish Hh pathway. We then addressed whether mouse Fu compensated for loss of zebrafish Fu. Surprisingly, co-injection of mouse *Fu* messenger RNA and zebrafish *fu* morpholino rescued all Hh phenotypes, including restoration of *ptc1* expression, lateral floor plate formation, muscle pioneer differentiation and somite shape (Fig. 2c, f, i, l, o, Supplementary Fig. 5 and data not shown). In contrast, co-injection of *Drosophila fu* mRNA and the zebrafish *fu* morpholino failed to rescue Hh phenotypes (data not shown). Thus, mouse Fu retains the necessary information to participate in the fish Hh pathway, indicating that a common mechanism underlies critical aspects of Hh signalling and motile ciliogenesis.

Fu may have an ancient, conserved role in regulating microtubule or motile cilia function because the genomes of many organisms, including plants and flagellated unicellular eukaryotes, contain genes encoding a highly conserved Fu kinase domain[21] (Supplementary Fig. 8). To test this idea, we examined *Fu* expression in different species by *in situ* hybridization and found strong expression in the chick tracheal epithelium and the oviduct and testis of *Xenopus tropicalis* (Fig. 3a, b and data not shown), in a pattern similar to mouse *Fu*. We then focused on zebrafish, which use 9+2 motile cilia on the surface of Kupffer's vesicle to generate a anticlockwise flow essential for establishment of left–right asymmetry[22]. If zebrafish Fu also participates in 9+2 cilia biogenesis, we reasoned that left–right asymmetry would be disrupted. We examined the positioning of the heart and visceral organs by *cardiac myosin light chain 2* (*cmlc2*, also known as *myl7*) and *fork head domain protein 2* (*fkd2*, also known as *foxa3*) expression, respectively. In contrast to zebrafish *smo* mutants, in which disrupted Hh signalling does not perturb left–right asymmetry[20] (Fig. 3c), 41% of *fu* morphants had reversed or midline hearts (Fig. 3d–f), whereas 30% of injected embryos had abnormal positioning of the gut, liver and pancreas (Supplementary Fig. 11). To investigate whether Fu is required for the early establishment of asymmetric gene expression in the left lateral plate mesoderm, we studied the expression pattern of *southpaw* (*spaw*) and *paired-like homeodomain transcription factor 2* (*pitx2*) in *fu* morphants. In 73% of *fu* morphants, *spaw* was found to be on the right side, bilateral, or absent in the lateral plate mesoderm (Fig. 3g–i). Similarly, 71% of *fu* morphants had markedly reduced or absent *pitx2* staining in the lateral plate mesoderm (data not shown). Co-injection of mouse *Fu*, but not *Drosophila fu*, with *fu* morpholino was sufficient to restore left–right asymmetry (Fig. 3f, i and data not shown).

To confirm a direct role for Fu in regulating Kupffer's vesicle function, we injected fluorescein-labelled *fu* morpholino into dorsal forerunner cells[23], which migrate at the leading edge of the embryonic shield to produce Kupffer's vesicle. Forty-four per cent of embryos with a strong fluorescent signal in the dorsal forerunner cells developed cardiac laterality but not somite defects (data not shown), indicating that the knockdown of *fu* in Kupffer's vesicle accounts for the left–right asymmetry defects. Kupffer's vesicle cilia in *fu* morphants had disorganized axonemal structures, including loss and acquisition of extra central pair microtubules (Fig. 3j–l and data not shown), indicating a conserved role of vertebrate *Fu* in central pair construction. Loss of *fu* affected cilia motility as shown by injecting rhodamine-conjugated dextran beads into Kupffer's vesicle of *fu* morphants at the 8-somite stage (Supplementary Movies 7 and 8). Defects in establishing an anticlockwise flow in *fu* morphants were rescued by mouse *Fu* (Supplementary Movie 9). Taken together, the data strongly support a conserved, Hh-independent role of Fu in vertebrate 9+2 cilia biogenesis (Fig. 3p).

The process of central pair construction is poorly characterized and Fu is the first regulatory component known to control its assembly. To determine how Fu might control this process, we tested the ability of Fu to interact with Spag6 (also known as Pf16) and Spag16 (Pf20), evolutionarily conserved components of the central pair apparatus[24,25]. When expressed in HEK 293T cells, Fu–Flag efficiently co-immunoprecipitated Spag16–haemagglutinin (HA), but not Spag6–HA (Fig. 4a). Notably, Spag16 localizes to the sperm central pair apparatus[26], and its *Chlamydomonas* orthologue Pf20 decorates the C2 microtubule along the intermicrotubule bridges between central pair microtubules[27]. This suggests a direct role for Fu in the assembly or maintenance of the central pair apparatus.

In fly, Fu binds to the kinesin Cos2 to transduce the Hh signal downstream of Smo. We examined whether mouse Fu bound to the mouse Cos2 orthologues Kif7 and Kif27. When expressed in HEK 293T cells and mouse tracheal epithelial cells (MTECs), Fu–Flag bound strongly to Kif27–Myc, but not to Kif7–Myc (Fig. 4b and data not shown), implicating Kif27 in the generation or regulation of 9+2 cilia. We expressed Kif27–green fluorescent protein (GFP) in MTECs by lentiviral infection and assessed its localization throughout MTEC

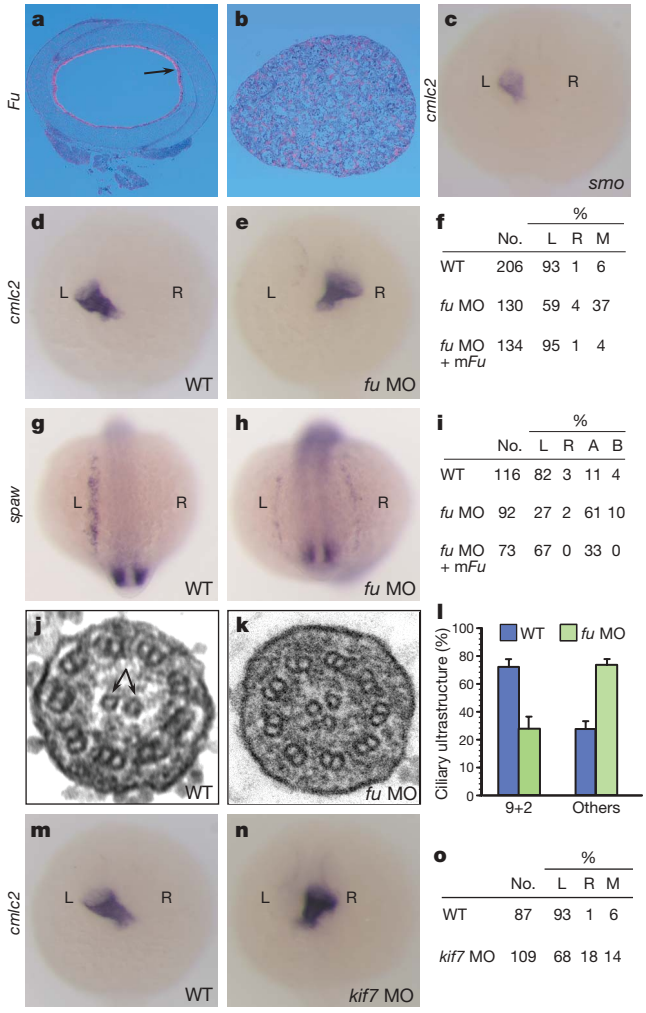

Figure 3 | Zebrafish *fu* has a Hh-independent role in left–right asymmetry and generation of 9+2 cilia. **a**, **b**, Section *in situ* hybridization to mouse *Fu* (pink signal) in chick trachea (**a**) and *X. tropicalis* testis (**b**). Arrow indicates sites of *Fu* expression. **c**, Whole mount *in situ* hybridization to *cmlc2* (purple signal) in $smo^{hi1640Tg}$ fish embryos at 24 h.p.f. View is dorsal. L, left; R, right. **d**, **e**, Whole-mount *in situ* hybridization to *cmlc2* in wild-type (**d**) and *fu* morphants (MO; **e**) at 24 h.p.f. View is dorsal. **f**, Summary of cardiac laterality defects in wild type ($n = 206$), *fu* morphants ($n = 130$), and *fu* morphants rescued with mouse *Fu* ($n = 134$). M, medial. **g**, **h**, Whole mount *in situ* hybridization to *spaw* at the 15-somite stage. View is dorsal. **i**, Summary of *spaw* expression in the lateral plate mesoderm in wild type ($n = 116$), *fu* morphants ($n = 92$), and *fu* morphants rescued with mouse *Fu* ($n = 73$). A, absent; B, bilateral. **j**, **k**, Electron micrograph of Kupffer's vesicle cilia from wild type (**j**) and a *fu* morphant (**k**). **l**, Quantification of ultrastructural defects in Kupffer's-vesicle cilia from wild type and *fu* morphants. Error bars indicate s.d. **m**, **n**, Whole mount *in situ* hybridization to *cmlc2* in wild-type and *kif7* morphants at 24 h.p.f. View is dorsal. **o**, Summary of cardiac laterality defects in wild-type ($n = 87$) and *kif7* morphants ($n = 109$). **p**, Summary of essential Fu, Cos2 and Kif27 functions in metazoan model organisms. Original magnification, ×40 (**a**, **b**), ×80 (**c**–**e**, **m**, **n**), ×105.6 (**g**, **h**) and ×100,000 (**j**, **k**).

differentiation induced by the creation of an air-liquid interface. During this process, hundreds of centrioles migrate to the apical surface of the cell, dock with the membrane to form basal bodies, and act as templates for the outgrowth of the outer microtubule doublets of the ciliary axoneme[28]. At air-liquid interface days 0 and

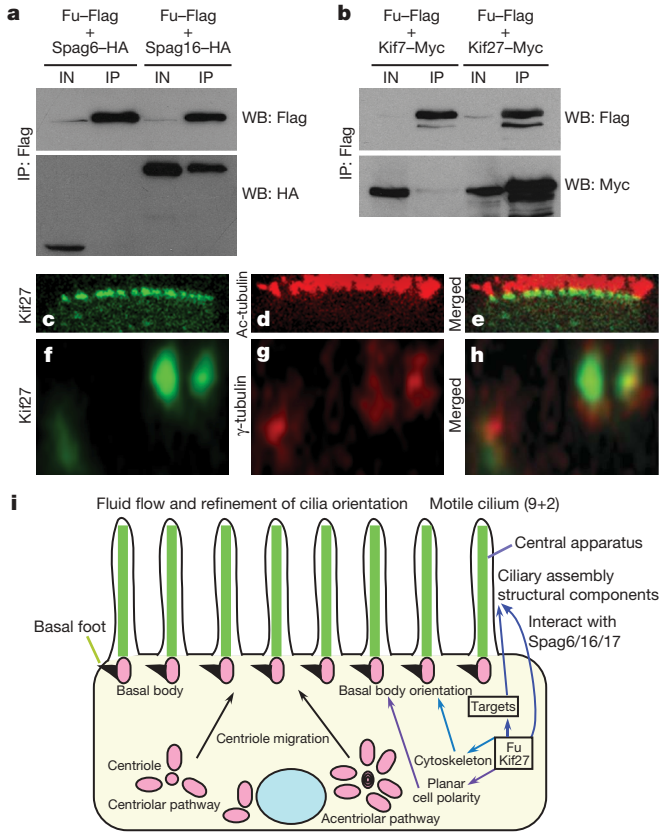

Figure 4 | Mouse Fu interacts with the central pair protein Spag16 and the Cos2 orthologue Kif27. **a**, Western blot of immunoprecipitated mouse Fu–Flag to detect its physical interaction with mouse Spag6–HA or Spag16–HA from HEK 293T lysates. IN, input; IP, immunoprecipitation; WB, western blot. **b**, Western blot of immunoprecipitated mouse Fu–Flag to determine its physical association with mouse Kif7–Myc or Kif27–Myc from HEK 293T lysates. **c–h**, Confocal images of fully differentiated MTECs to visualize localization of Kif27–GFP to the basal body (marked by anti-γ-tubulin) of motile cilia labelled with acetylated tubulin (Ac-tubulin). **i**, Model of Fu, Kif27 and Spag16 function in motile cilia construction. Original magnification, ×1,500 (**c–h**).

5, Kif27–GFP punctae were associated with centrioles as determined by γ-tubulin staining (Supplementary Fig. 6). Kif27–GFP associated with the base of the cilium after axoneme outgrowth (Fig. 4c–h). Fu–mCherry was broadly distributed in the cytoplasm of MTECs throughout differentiation, overlapping with Kif27 (Supplementary Fig. 6). *Fu* and *Kif27* expression are upregulated during MTEC differentiation, consistent with their essential roles in motile ciliogenesis (Supplementary Fig. 7). Efforts to demonstrate Fu kinase activity *in vitro* have not been successful, suggesting the requirement of a special microenvironment for its activity. We speculate that Fu has several substrates, some of which could reside in the cytoplasm and control central pair assembly indirectly (Fig. 4i). Our data favour a model in which Kif27 and/or Spag16 directs the localization or activity of Fu for central pair construction (Fig. 4i).

Despite the non-essential role of Fu in mammalian Hh signalling, the protein retains an interaction with the Cos2 orthologue Kif27. Analysis of Cos2, Kif7 and Kif27 sequences indicates that the *Kif7* and *Kif27* genes may have arisen by a duplication event (Supplementary Fig. 9). The four fish species examined do not contain an obvious Kif27 orthologue, suggesting either that Kif27 was lost after gene duplication, or that the duplication event occurred after divergence of the fish and amphibian lineages. Supporting the latter, morpholino knockdown of *kif7* in zebrafish (z) resulted in both Hh-specific phenotypes and disruption of left–right asymmetry (Fig. 3m–o and data not shown), indicating a dual role for Kif7 in Hh signalling[29] and motile ciliogenesis, similar to zFu which co-immunoprecipitates with zKif7 (Supplementary Fig. 12). There are conflicting reports on the roles of Kif7 and Kif27 in vertebrate Hh signalling[29,30]; on the basis of data here, we predict that Kif27 does not have a vital role in mammalian Hh signal transduction, and mice lacking functional Kif27 may have phenotypes similar to Fu. We speculate that Fu has evolved or retained its function in central pair assembly in vertebrates, and that duplication of ancestral Cos2 in the vertebrate lineage led to the partition of functions for Kif7 and Kif27, while Kif27 retained its partnership with Fu (Fig. 3p). Although the requirement of Fu-like activity in mammalian Hh signalling is unproven, if it exists it is probably compensated for by an unrelated kinase (Supplementary Fig. 8). Alternatively, the involvement of the primary cilium as a scaffold for Hh pathway components in mammals could circumvent the need for a Fu–kinesin complex. Consistent with the notion of evolutionary changes in Hh pathway design in different species, Su(fu), a component of the cytoplasmic signalling complex, is dispensable for fly viability, plays a minor role in zebrafish Hh signalling and becomes an important negative regulator in mice[2]. Further analysis of Fu and Kif27 function in ciliogenesis and Hh signalling in diverse species will provide further insight into the evolution of this critical signalling pathway.

METHODS SUMMARY

Transmission electron microscopy. Mouse tissue was fixed in 3% glutaraldehyde, 1% paraformaldehyde, 0.1 M sodium cacodylate, pH 7.4, at 4 °C overnight. Fish embryos were fixed in 2% paraformaldehyde, 2% glutaraldehyde (electron-microscopy grade) at room temperature for 2 h. Standard processing, embedding and sectioning procedures were followed. Samples were examined on a JEOL 100CX or JEM-1230 transmission electron microscope.

Basal foot polarity. The orientation and circular standard deviation of basal feet in electron microscopy micrographs was calculated as described[18]. Circular statistics were calculated using Oriana 2.0 (Kovachs Computing Services).

Tracheal flow assays. Tracheae from P14 wild-type and $Fu^{-/-}$ mice were excised, cleaned of muscle and vasculature, opened longitudinally, and placed in a drop of PBS on a glass slide. Five microlitres of a 0.01% solution of Fluospheres (Invitrogen) were added on top of a single trachea to visualize the direction of ciliary flow. Images were acquired using a SPOT 2.3 camera connected to a Nikon E1000 epifluorescence microscope. Images were captured at a rate of 26 frames per second (f.p.s.) over a 50 μm × 50 μm area and were saved as .tiff stacks. Movies were examined in NIH Image J using the enhancing feature of the SpotTracker plugin (D. Sage and S. Gasser) to optimize sphere intensity, and the MtrackJ plugin (E. Meijering, Biomedical Imaging Group, University Medical Center, Rotterdam) to trace the direction and path length of the sphere. Average velocity was taken to be the straight-line distance a particle travelled from its originating point divided by time, and was calculated in Microsoft Excel.

Full Methods and any associated references are available in the online version of the paper at www.nature.com/nature.

Received 10 September 2008; accepted 10 February 2009.
Published online 22 March 2009.

1. McMahon, A. P., Ingham, P. W. & Tabin, C. J. Developmental roles and clinical significance of hedgehog signaling. *Curr. Top. Dev. Biol.* **53**, 1–114 (2003).
2. Huangfu, D. & Anderson, K. V. Signaling from Smo to Ci/Gli: conservation and divergence of Hedgehog pathways from *Drosophila* to vertebrates. *Development* **133**, 3–14 (2006).
3. Sisson, J. C., Ho, K. S., Suyama, K. & Scott, M. P. Costal2, a novel kinesin-related protein in the Hedgehog signaling pathway. *Cell* **90**, 235–245 (1997).
4. Robbins, D. J. *et al.* Hedgehog elicits signal transduction by means of a large complex containing the kinesin-related protein costal2. *Cell* **90**, 225–234 (1997).
5. Lum, L. *et al.* Hedgehog signal transduction via Smoothened association with a cytoplasmic complex scaffolded by the atypical kinesin, Costal-2. *Mol. Cell* **12**, 1261–1274 (2003).
6. Chen, M. H., Gao, N., Kawakami, T. & Chuang, P. T. Mice deficient in the fused homolog do not exhibit phenotypes indicative of perturbed hedgehog signaling during embryonic development. *Mol. Cell. Biol.* **25**, 7042–7053 (2005).
7. Merchant, M. *et al.* Loss of the serine/threonine kinase fused results in postnatal growth defects and lethality due to progressive hydrocephalus. *Mol. Cell. Biol.* **25**, 7054–7068 (2005).
8. Katoh, Y. & Katoh, M. KIF27 is one of orthologs for *Drosophila* Costal-2. *Int. J. Oncol.* **25**, 1875–1880 (2004).

9. Davenport, J. R. & Yoder, B. K. An incredible decade for the primary cilium: a look at a once-forgotten organelle. *Am. J. Physiol. Renal Physiol.* **289,** F1159–F1169 (2005).
10. Davis, E. E., Brueckner, M. & Katsanis, N. The emerging complexity of the vertebrate cilium: new functional roles for an ancient organelle. *Dev. Cell* **11,** 9–19 (2006).
11. Afzelius, B. A. Cilia-related diseases. *J. Pathol.* **204,** 470–477 (2004).
12. Marshall, W. F. & Kintner, C. Cilia orientation and the fluid mechanics of development. *Curr. Opin. Cell Biol.* **20,** 48–52 (2008).
13. Zariwala, M. A., Knowles, M. R. & Omran, H. Genetic defects in ciliary structure and function. *Annu. Rev. Physiol.* **69,** 423–450 (2007).
14. McKean, P. G., Baines, A., Vaughan, S. & Gull, K. γ-Tubulin functions in the nucleation of a discrete subset of microtubules in the eukaryotic flagellum. *Curr. Biol.* **13,** 598–602 (2003).
15. Chilvers, M. A., Rutman, A. & O'Callaghan, C. Ciliary beat pattern is associated with specific ultrastructural defects in primary ciliary dyskinesia. *J. Allergy Clin. Immunol.* **112,** 518–524 (2003).
16. Yang, X., Dillon, R. H. & Fauci, L. J. An integrative computational model of multiciliary beating. *Bull. Math. Biol.* **70,** 1192–1215 (2008).
17. Frisch, D. & Farbman, A. I. Development of order during ciliogenesis. *Anat. Rec.* **162,** 221–232 (1968).
18. Mitchell, B., Jacobs, R., Li, J., Chien, S. & Kintner, C. A positive feedback mechanism governs the polarity and motion of motile cilia. *Nature* **447,** 97–101 (2007).
19. Wolff, C., Roy, S. & Ingham, P. W. Multiple muscle cell identities induced by distinct levels and timing of hedgehog activity in the zebrafish embryo. *Curr. Biol.* **13,** 1169–1181 (2003).
20. Chen, W., Burgess, S. & Hopkins, N. Analysis of the zebrafish smoothened mutant reveals conserved and divergent functions of hedgehog activity. *Development* **128,** 2385–2396 (2001).
21. Oh, S. A. *et al.* A divergent cellular role for the FUSED kinase family in the plant-specific cytokinetic phragmoplast. *Curr. Biol.* **15,** 2107–2111 (2005).
22. Kramer-Zucker, A. G. *et al.* Cilia-driven fluid flow in the zebrafish pronephros, brain and Kupffer's vesicle is required for normal organogenesis. *Development* **132,** 1907–1921 (2005).
23. Shu, X. *et al.* Na,K-ATPase α2 and Ncx4a regulate zebrafish left-right patterning. *Development* **134,** 1921–1930 (2007).
24. Neilson, L. I. *et al.* cDNA cloning and characterization of a human sperm antigen (SPAG6) with homology to the product of the Chlamydomonas PF16 locus. *Genomics* **60,** 272–280 (1999).
25. Sapiro, R. *et al.* Sperm antigen 6 is the murine homologue of the *Chlamydomonas reinhardtii* central apparatus protein encoded by the *PF16* locus. *Biol. Reprod.* **62,** 511–518 (2000).
26. Zhang, Z. *et al.* A sperm-associated WD repeat protein orthologous to *Chlamydomonas* PF20 associates with Spag6, the mammalian orthologue of *Chlamydomonas* PF16. *Mol. Cell. Biol.* **22,** 7993–8004 (2002).
27. Smith, E. F. & Lefebvre, P. A. PF20 gene product contains WD repeats and localizes to the intermicrotubule bridges in Chlamydomonas flagella. *Mol. Biol. Cell* **8,** 455–467 (1997).
28. Dawe, H. R., Farr, H. & Gull, K. Centriole/basal body morphogenesis and migration during ciliogenesis in animal cells. *J. Cell Sci.* **120,** 7–15 (2007).
29. Tay, S. Y., Ingham, P. W. & Roy, S. A homologue of the *Drosophila* kinesin-like protein Costal2 regulates Hedgehog signal transduction in the vertebrate embryo. *Development* **132,** 625–634 (2005).
30. Varjosalo, M., Li, S. P. & Taipale, J. Divergence of hedgehog signal transduction mechanism between *Drosophila* and mammals. *Dev. Cell* **10,** 177–186 (2006).

Supplementary Information is linked to the online version of the paper at www.nature.com/nature.

Acknowledgements We thank H. Bourne, C. C. Hui, Z. Zhang, J. Strauss III and W. Hwang for constructs, antibodies and sharing of unpublished results; R. Harland and T. Mikawa for *X. tropicalis* and chicken tissue; K. Thorn and S. Dandekar for assistance with microscopy and ciliary beat frequency analysis; M.-L. Cheong and Y. Nozawa for technical assistance; and D. Casso, S. Coughlin, T. Kornberg, W. Marshall, T. Mikawa, K. Wemmer and members of the Chen and Chuang laboratories for discussion and critical reading of the manuscript. Some data for this study were acquired at the Nikon Imaging Center at UCSF/QB3. This work was supported by grants from the National Institutes of Health to J.-N.C. and P.-T.C., and a Career Investigator Award from the American Lung Association to P.-T.C.

Author Information Reprints and permissions information is available at www.nature.com/reprints. Correspondence and requests for materials should be addressed to P.-T.C. (pao-tien.chuang@ucsf.edu).

METHODS

Animal husbandry. $Fu^{+/-}$ mice were maintained as described[6]. Wild-type AB fish were used and raised as described[31]. The *smoothened* (also known as *slow muscle omitted*) allele[20] used in this study is $smo^{hi1640Tg}$.

Molecular biology. Standard molecular biology techniques, including molecular cloning, genomic DNA preparation, RNA isolation, PCR, RT–PCR and Southern analysis were performed as described[32,33]. Fu–Flag, Fu–4×Flag, Fu–mCherry, Kif7–3×Myc, Kif27–3×Myc, Kif27–GFP, SPAG16L–3×HA, and SPAG6–3×HA were cloned into pCAGGS (for immunoprecipitation and immunofluorescence in mammalian cells), pCS2+ (for expression in zebrafish), pcDNA3 (for immunoprecipitation and immunofluorescence in mammalian cells), or FuPw (for lentiviral expression) vectors. Detailed methods and maps are available on request.

FuPw vector (courtesy of K. Wong and H. Bourne) contains the HIV-1 flap sequence, the human polyubiquitin C promoter, a multiple cloning site, and the woodchuck hepatitis virus post-transcriptional regulatory element. Flanking this cassette are 5′ and 3′ self-inactivating long-terminal repeats. Expression constructs were co-transfected with the HIV packaging vector pCMVΔ8,9 and the envelope glycoprotein vector pVSV-G into HEK293T cells using Lipofectamine 2000 (Invitrogen).

Morpholino injections. Wild-type zebrafish embryos were injected with 1.6–4 ng *fu* or 8–12 ng *kif7* or 0.2 ng *ptc1* MO at the one- to two- cell stage. Fluorescein-tagged *fu* morpholino (4 ng) was injected into the yolk of 128-cell-stage embryos to target dorsal forerunner cells. A *p53* morpholino was co-injected with *fu* or *kif7* morpholino at the same concentration to block nonspecific cell death[34]. In rescue experiments, 400 pg of mouse *Fu* mRNA was co-injected with *fu* morpholino. In testing genetic epistasis, 0.2 ng of *ptc1* and 2 ng of *fu* MO were co-injected. The *fu* (5′-TGGTACTGATCCATCTCCAG CGACG-3′), *kif7* (5′-GCCGACTCCTTTTGGAGACATAGCT-3′) and *ptc1* MO (5′-CATAGTCCAAACGGGAGGCAGAAGA-3′) were described previously[19].

***In situ* hybridization.** Histological analysis and section *in situ* hybridization using ^{33}P-labelled riboprobes were performed as described[6]. Probes for chick, zebrafish and *X. tropicalis Fu* were amplified by PCR using partial or full-length cDNAs (Open Biosystems) as templates. Zebrafish embryos were raised in medium treated with 0.2 mM 1-phenyl-1-2-thiourea to maintain optical transparency. Whole mount *in situ* hybridization was performed as described[35]; probes used were *cmlc2*, *fkd2*, *fkd4*, *nkx2.2b*, *fused*, *shh*, *ptc1*, *spaw* and *pitx2*.

Ciliary beat frequency and waveform measurements. Tracheae were dissected out from P10–P14 wild-type and $Fu^{-/-}$ animals, and cut into rings or strips. Tracheae were washed briefly in PBS and placed in DMEM supplemented with 10% FBS, penicillin–streptomycin and L-glutamate. Tissue was placed in a few drops of medium in a 35-mm glass bottom microwell dish (MatTek). Cilia beating was observed using DIC microscopy on a Nikon TE2000E inverted microscope equipped with Perfect Focus, a ×60 water immersion objective, ×1.5 zoom adaptor and an *in vivo* Scientific incubator set at 37 °C and 5% CO_2. A Photometrics Coolsnap HQ2 camera and NIS Elements 2.3 software were used to acquire videos of beating cilia at frame rates of 60–70 f.p.s., depending on the size of the defined region of interest (ROI). Ciliary beat frequency was measured by defining an ROI in the upper third of the ciliary shaft, and plotting the changes in pixel intensity over time in the obtained image series. This data was subsequently Fourier transformed to obtain the frequency using MatLab. Waveform was analysed by tracing of cilia from individual movie frames in Adobe Illustrator, or by manual tracking using the MtrackJ plugin (E. Meijering, Biomedical Imaging Group, University Medical Center, Rotterdam) in NIH ImageJ.

Cell culture, transfections and immunoprecipitation. HEK 293T cells were maintained in DMEM supplemented with 10% FBS, penicillin–streptomycin and L-glutamate. Cells were transfected with Lipofectamine 2000 (Invitrogen) according to manufacturer's instructions. Forty-eight hours after transfection, cells were collected and lysed in lysis buffer (1% Triton X-100, 150 mM NaCl, 50 mM Tris-HCl, pH 7.5, 1 mM EDTA, 0.5 mM PMSF, 2 μg ml^{-1} pepstatin A, 10 μg ml^{-1} leupeptin, 5 μg ml^{-1} aprotinin). Lysates were sheared with a 20-gauge needle and remained on ice for 30 min. Lysates were then clarified by centrifugation at 20,817*g* for 20 min at 4 °C. The supernatant was removed and bound to 50 μl of anti-Flag M2 agarose beads (Sigma) for 4 h at 4 °C with constant nutation. Beads were washed five times with lysis buffer before the addition of sample buffer. Immunoprecipitated proteins were analysed by 7.5% SDS–PAGE and transferred to PVDF for immunoblotting. Antibodies used were rabbit anti-Flag (Sigma, 1:2,000), rabbit anti-Myc (Sigma, 1:2,000), and rabbit anti-HA (Sigma, 1:1,000).

Primary MTEC culture and viral transduction. Primary MTECs were derived from P10–P21 mice and cultured as described[36]. Lentivirus was produced by co-transfecting cDNAs cloned into the FuPw vector with pCMVΔ8,9 and pVSV-G into HEK 293T cells as described above. Supernatant was collected 72–96 h after transfection, filtered through a 0.45 μm PES membrane syringe filter unit (Nalgene), and concentrated tenfold using a Centriprep Ultracel YM-10 device (Millipore). Infection of MTECs was performed as described[37].

Immunofluorescence and microscopy. Cells were fixed in 4% paraformaldehyde for most applications, or in ice-cold methanol for visualization of basal bodies. Standard procedures were used for immunostaining. Primary antibodies used were mouse anti-acetylated-α-tubulin (Sigma, 1:2,000) and mouse anti-γ tubulin (Sigma, 1:2,000). Secondary antibodies and conjugates used were donkey anti-mouse AlexaFluor 594 (Molecular Probes, 1:2,000), donkey anti-mouse FITC (Molecular Probes, 1:2,000), and rhodamine-conjugated phalloidin (Sigma, 1:200). Fluorescent confocal images were acquired using a Nikon TE2000U inverted microscope with a Yogokawa CSU22 spinning disk confocal (Solamere Technology Group), a Photometrics Cascade II Camera, and MicroManager software (Vale laboratory, University of California–San Francisco). Images were acquired with a ×100 oil-immersion lens and a ×1.5 zoom adaptor (Nikon) using two laser lines (488 nm and 568 nm). Confocal stacks were collected using a 0.25-μm step size along the *z*-axis. Stacks were analysed and *xy*, *xz*, and *yz* projections were generated using ImageJ and the VolumeViewer plugin (K. U. Barthel, Internationale Medieninformatik). Deconvolution was performed with the Iterative Deconvolve 3D plugin (R. Dougherty, OptiNav, Inc.).

Immunohistochemistry staining. Immunohistochemistry staining using anti-Engrailed (4D9, Developmental Studies Hybridoma Bank) at 1:100 dilution and anti-acetylated tubulin (Sigma) at 1:200 dilution was conducted as described[23]. Confocal images were acquired with an LSM510 confocal microscope (Zeiss).

Fluorescent bead injection. Fluorescent beads diluted 1:100 in PBS were injected into Kupffer's vesicle at the 8–10-somite stage[23]. Embryos were imaged on a Zeiss Axioplan 2 microscope using a ×63 water immersion lens (Zeiss).

31. Westerfield, M. *The Zebrafish Book* (Univ. Oregon Press, 1995).
32. Nagy, A., Gertsenstein, M., Vintersten, K. & Behringer, R. *Manipulating the Mouse Embryo: A Laboratory Manual* 3rd edn (Cold Spring Harbour Laboratory Press, 2003).
33. Sambrook, J. & Russell, D. W. *Molecular Cloning: A Laboratory Manual* (Cold Spring Harbour Laboratory Press, 2001).
34. Eisen, J. S. & Smith, J. C. Controlling morpholino experiments: don't stop making antisense. *Development* **135,** 1735–1743 (2008).
35. Chen, J. N. & Fishman, M. C. Zebrafish tinman homolog demarcates the heart field and initiates myocardial differentiation. *Development* **122,** 3809–3816 (1996).
36. You, Y., Richer, E. J., Huang, T. & Brody, S. L. Growth and differentiation of mouse tracheal epithelial cells: selection of a proliferative population. *Am. J. Physiol. Lung Cell. Mol. Physiol.* **283,** L1315–L1321 (2002).
37. Vladar, E. K. & Stearns, T. Molecular characterization of centriole assembly in ciliated epithelial cells. *J. Cell Biol.* **178,** 31–42 (2007).